2132 *Inorg. Chem.* **2010**, *49*, 2132–2140
DOI: 10.1021/ic901737y

Inorganic Chemistry
Article

Structural and Dynamical Aspects of the Unsymmetric Hydration of Sb(III): An ab initio Quantum Mechanical Charge Field Molecular Dynamics Simulation

Len Herald V. Lim, Anirban Bhattacharjee, S. Sikander Asam, Thomas S. Hofer, Bernhard R. Randolf, and Bernd M. Rode*

Theoretical Chemistry Division, Institute of General, Inorganic, and Theoretical Chemistry, University of Innsbruck, Innrain 52a, A-6020 Innsbruck, Austria

Received September 1, 2009

An ab initio quantum mechanical charge field molecular dynamics (QMCF MD) simulation was performed to investigate the behavior of the Sb^{3+} ion in aqueous solution. The simulation reveals a significant influence of the residual valence shell electron density on the solvation structure and dynamics of Sb^{3+}. A strong hemidirectional behavior of the ligand binding pattern is observed for the first hydration shell extending up to the second hydration layer. The apparent domain partitioned structural behavior was probed by solvent reorientational kinetics and three-body distribution functions. The three-dimensional hydration space was conveniently segmented such that domains having different properties were properly resolved. The approach afforded a fair isolation of localized solvent structural and dynamical motifs that Sb^{3+} seems to induce to a remarkable degree. Most intriguing is the apparent impact of the lone pair electrons on the second hydration shell, which offers insight into the mechanistic aspects of hydrogen bonding networks in water. Such electronic effects observed in the hydration of Sb^{3+} can only be studied by applying a suitable quantum mechanical treatment including first and second hydration shell as provided by the QMCF ansatz.

1. Introduction

Knowledge of the behavior of antimony and its ions in aqueous solution is crucial for the understanding of its impact on the environment and the optimization of its removal from drinking water. Traditionally, antimony was used in lead−antimony alloys. Antimony is highly consumed in the battery industry, and its most common compound (Sb_2O_3) is used in flame retardants, catalysts, ceramics, glasses, and pigments, but it mostly cannot be recycled and is thus released directly into the environment.[1] Antimony production has steadily increased, and its use has changed over the years. Antimonial drugs are currently the first-line drugs for the treatment of leishmaniasis[2] while recently the pentavalent antimonials were also found to exert activity in experimental models of cancer, hepatitis C, and HIV.[3] Structure and dynamics of various ions have already been investigated by a large number of experimental and theoretical studies.[4−7] To our best knowledge no simulation data has been reported on the structure and dynamics of Sb^{3+} in aqueous solution.

The description of hydration processes of ions with a lone electron pair such as Ge^{2+} [8,9] and Sn^{2+} [10] yielded very interesting insight into their hemidirectional ligand binding behavior in aqueous solution. In this context, it was of interest to explore if a similar coordination pattern would be observed for a cationic species isoelectronic with Sn^{2+}, but possessing a higher charge, thus motivating the present study of Sb^{3+} in aqueous solution. To probe such complex electronic effects, an accurate quantum mechanical treatment is mandatory.

Concurrent developments in computer speed and capacity have paved the way for simulation techniques using combined ab initio quantum mechanical and molecular mechanical (QM/MM) simulations, and the recently developed quantum mechanical charge field molecular dynamics (QMCF MD) approach[11] has been found to be suitable for the study of composite and asymmetrically hydrated ions,

*To whom correspondence should be addressed. E-mail: bernd.m.rode@uibk.ac.at. Phone: +43-512-507-5160. Fax: +43-512-507-2714.

(1) Quentel, F.; Filella, M.; Elleouet, C.; Madec, C.-L. *Environ. Sci. Technol.* **2004**, *38*, 2843–2848.
(2) Berman, J. *Curr. Opin. Infect. Dis.* **2003**, *16*, 397–401.
(3) Yan, S.; Jin, J.; Sun, H.; Gielen, M.; Tiekink, E. R. *Metallotherapeutic Drugs and Metal-Based Diagnostic Agents: The Use of Metals in Medicine*. John Wiley and Sons: New York, 2005.
(4) Ohtaki, H.; Radnai, T. *Chem. Rev.* **1993**, *93*(3), 1157–1204.
(5) Helm, L.; Merbach, A. E. *Chem. Rev.* **2005**, *105*, 1923.
(6) Helm, L.; Merbach, A. E. *J. Chem. Soc., Dalton Trans.* **2002**, 633–641.
(7) Rode, B. M.; Schwenk, C.; Hofer, T.; Randolf, B. *Chem. Rev.* **2005**, *249*(24), 2993–3006.
(8) Azam, S. S.; Hofer, T. S.; Randolf, B. R.; Rode, B. M. *Chem. Phys. Lett.* **2009**, *470*, 85–89.
(9) Azam, S. S.; Lim, L. H. V.; Hofer, T. S.; Randolf, B. R.; Rode, B. M. *J. Comput. Chem.* **2009**, *31*, 278−285.
(10) Lim, L. H. V.; Hofer, T. S.; Pribil, A. B.; Rode, B. M. *J. Phys. Chem. B* **2009**, *113*(13), 4372–4378.
(11) Rode, B. M.; Hofer, T. S.; Randolf, B. R.; Schwenk, C. F.; Xenides, D.; Vchirawongkwin, V. *Theor. Chim. Acta* **2006**, *115*, 77–85.

 Published on Web 02/02/2010

mainly because of the inclusion of both primary and secondary hydration layers in the QM treatment. The present work aims at eludicating the hydration behavior of Sb^{3+} paying close attention to solvent reorganizational patterns and dynamics, and how these are affected by the presence of the lone electron pair. The results are later discussed in relation to selected antimony compounds/complexes from which some generalizations on the stereochemical activity of the lone electron pair can be derived.

2. Methods

For an accurate estimation of the method of choice, geometry optimizations of $[Sb(H_2O)_{n=1-8}]^{3+}$ clusters were performed employing different levels of theory using cc-pvdz-PP [12] basis set for Sb and Dunning double-ζ plus polarization basis sets[13] for O and H which have successfully been applied in previous investigations.[14−16] Energy values of B3LYP are differing considerably from the MP2 and CCSD values, while the Hartree−Fock (HF) level resulted in energy values within a range of 0.5 kcal/mol in relation to those of CCSD and MP2 calculations as shown in Table 1. Fair agreement between the different levels, however, can be seen in the average Sb−O bond distances obtained from the optimized $[Sb(H_2O)_{n=1-8}]^{3+}$ cluster geometries (Table 2). As neither MP2 nor CCSD is computationally affordable for a simulation at present, the HF level of theory was chosen as a reasonable compromise for the QM calculation of forces.

Similar to standard QM/MM, the QMCF framework utilizes a partitioning scheme for applying quantum mechanical and molecular mechanical levels of theory. The major difference is in how the QMCF methodology treats forces between the core region and the MM region. Because of the relatively large QM radius, only the Coloumbic forces become significant in describing the interaction of the solvent with the solute. The enlarged distance between any solvent molecules in the MM region and the solute removes the need for the construction of classical potentials as the corresponding non-Coloumbic interactions become negligibly small. A layer zone inside the QM region provides an intermediary mechanism for coupling QM and MM generated forces for particles transiting between regions. Force switching is applied over a small smoothing layer at the onset of the MM zone using the equation:

$$S(r) = 1, \quad \text{for} \quad r \le r_1$$

$$S(r) = \frac{(r_0^2 - r^2)^2(r_0^2 + 2r^2 - 3r_1^2)}{(r_0^2 - r_1^2)^3}, \quad \text{for} \quad r_1 < r \le r_0 \quad (1)$$

$$S(r) = 0, \quad \text{for} \quad r > r_0$$

where r_0 and r_1 define the lower and upper radial bounds of the smoothing layer, respectively. The transition force then becomes:

$$F_J^{\text{Smooth}} = S(r) \cdot (F_J^{\text{layer}} - F_J^{\text{MM}}) + F_J^{\text{MM}} \quad (2)$$

Table 1. Average Binding Energies in kcal/mol for $[Sb(H_2O)_n]^{3+}$ Clusters, Obtained from HF, MP2, CCSD, and B3LYP Calculations

	E_{bond} in kcal/mol			
n	HF	MP2	CCSD	B3-LYP
1	−140.45	−140.46	−140.71	−160.24
2	−114.62	−114.67	−114.92	−132.59
3	−116.24	−116.37	−116.56	−127.46
4	−103.82	−103.98	−104.15	−113.14
6	−85.86	−85.96	−86.14	−92.74
8	−72.00	−72.06	−72.26	−77.77

Table 2. Average Sb−O Bond Lengths (in Å) for $[Sb(H_2O)_n]^{3+}$ Clusters, Obtained from HF, MP2, CCSD, and B3LYP Calculations

	E_{bond} in kcal/mol			
n	HF	MP2	CCSD	B3-LYP
1	2.05	2.06	2.06	2.08
2	2.20	2.19	2.19	2.21
3	2.13	2.14	2.14	2.16
4	2.20	2.20	2.20	2.22
6	2.37	2.35	2.36	2.37
8	2.48	2.46	2.47	2.47

F_J^{layer} is the force derived by coupling QM and MM contributions in the layer zone. Differences between QMCF and standard QM/MM methods, and the advantages of the former have already been extensively discussed in previous publications,[11,17] demonstrating that the QMCF framework offers a straightforward route to access any kind of solutes such as metal complexes and even composite solute species.[18−22]

Because localized structural properties are often hidden in standard radial distribution functions, a scheme was used to decompose the diffuse hydration sphere of Sb^{3+}. The method involved a similar principle to that used in the study of the hydration of Sn(II),[10] but instead utilized Gaussian functions for the assignment of weights to ligand coordinates in the computation of the cluster centroid, Q. The scheme is based on the assumption that the full hydration volume of an ion can be represented as a concentric set of ligand distributions, each Gaussian in nature and having a corresponding mean ion-ligand distance, r. The computation can be performed with one Gaussian function, $f_g(r)$, representative of the highest ligand density, according to the equation:

$$Q = \sum f_g(r_i) \cdot R_i \quad (3)$$

where R_i represents the coordinates of ligand i. The centroid, Q, if made available for each frame of the trajectory, can be used to track the motion of the hydration volume and to generate spatially discriminated correlation subregions.

In addition, as all particle coordinates are available at each frame in the simulation trajectory, the local density corrected three-particle distribution function[23] was employed to

(12) Peterson, K. A.; Figgen, D.; Dolg, M.; Stoll, H. *J. Chem. Phys.* **2007**, *126*(12), 124101.
(13) Dunning, T. H., Jr. *J. Chem. Phys.* **1970**, *53*, 2823.
(14) Fatmi, M. Q.; Hofer, T. S.; Randolf, B. R.; Rode, B. M. *J. Chem. Phys.* **2005**, *123*, 4514–4521.
(15) Hofer, T. S.; Randolf, B. R.; Rode, B. M. *Phys. Chem. Chem. Phys.* **2005**, *7*, 1382–1387.
(16) Hofer, T. S.; Rode, B. M. *Chem. Phys.* **2005**, *312*, 81–88.
(17) Hofer, T. S.; Randolf, B. R.; Rode, B. M. *Solvation Effects on Molecules and Biomolecules*; Springer: Heidelberg, 2008.
(18) Hofer, T. S.; Shah, S. A. A.; Randolf, B. R.; Rode, B. M.; Persson, I. *Chem. Phys. Lett.* **2007**, *445*(4), 193–197.
(19) Rode, B. M.; Hofer, T. S. *Pure Appl. Chem.* **2006**, *78*(3), 525–539.
(20) Hofer, T. S.; Pribil, A. B.; Randolf, B. R.; Rode, B. M. *Chem. Phys.* **2008**, *349*(03), 182–185.
(21) Pribil, A. B.; Hofer, T. S.; Randolf, B. R.; Rode, B. M. *J. Comput. Chem.* **2008**, *29*(14), 2330–2334.
(22) Azam, S. S.; Hofer, T. S.; Randolf, B. R.; Rode, B. M. *J. Phys. Chem. A* **2009**, *113*(9), 1827–1834.
(23) Bhattacharjee, A.; Hofer, T. S.; Rode, B. M. *Phys. Chem. Chem. Phys.* **2008**, *10*, 6653–6657.

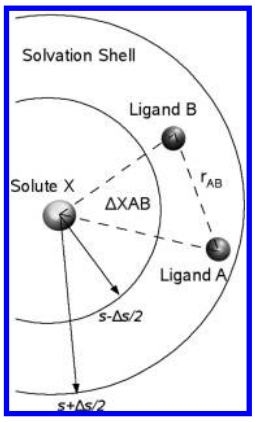

Figure 1. Scheme for probing local solvent structure reorganizations in terms of three body distributions $f^{(3)}_{X-O-O}(s, r, s)$.

observe solvent reorganizational patterns around the Sb^{3+} ion. The type of higher order correlation availed by this analysis is particularly suited for studying triangular co-disposition of particles from which certain organizational motifs can be deduced. Figure 1 illustrates the basic scheme of the analysis. Briefly, the three-particle distribution, $f^{(3)}_{X-O-O}(s, r, s)$, can be computed as:

$$f^{(3)}_{X-O-O}(s,r,s) = \frac{\langle N^{(3)}(s,r,s)\rangle}{8\pi^2 N_X \rho^2_{Shell} r s^2 \Delta s^2 \Delta r} \qquad (4)$$

where, $f^{(3)}_{X-O-O}(s, r, s)$ represents the local density corrected three-body distribution of ligand oxygens in a shell specified by $S \pm \Delta S/2$, and $\langle N^{(3)}(s, r, s)\rangle$ refers to the average number of triangular O−X−O configurations, whose O−O distance is r_{AB} recorded in a histogram bin of width Δr. The utility of this distribution function is most conveniently expressed in the comparison of patterns observed between solvated and pure solvent systems, as water molecules in neat water possess preferred configurational dispositions, facilitated by transient hydrogen bonds, that can be disrupted and reorganized in the presence of a strong charged solute. The resulting reorganizational response is a many-body effect that cannot be properly accounted for in standard pair correlations. With proper application of local density corrections to account for the non-homogeneity of ligand density around a solute, the local density corrected three-body distribution function can also be used to confirm the presence of weak hydration shells as in the case of aqueous Be^{2+} and U^{4+} solutions.[24,25] Its implications to the present study shall be emphasized further in the discussion of the results. A more thorough explanation of the underlying principles as well as illustrative sample applications can be seen in the original paper.[23]

Subsequently, solvent dynamics within and between hydration shells were analyzed via mean residence time calculations (using the direct method[26]) and the time correlation functions (TCF), $C_\mu(\tau)$[27,28] and $C_{HB}(\tau)$.[29−31] The upper-bounds for the parameter values of the latter were chosen as $R_{OH} = 2.5$ Å, $R_{OO} = 3.3$ Å, and $\theta = 25°$, based on neat water classical simulations using the BJH−CF2 model.[32,33] The TCFs, when related to their corresponding decay constants, provide a measure of their rates of relaxation. For the purpose of simplifying the intepretation of decay constants, the long time section of the decay curves were fitted to a single exponential. In this work, the relaxation constants of the dipole correlation function, τ_μ, and of the intermittent hydrogen bond, τ_{HB}, were computed for the first and second hydration shells in both total and partial (hemispherical) cases.

To characterize the structure of the lone electron pair on Sb^{3+}, representative structures formed in the course of the simulation (solute + first shell ligands) were taken for the analysis of the HF molecular orbitals (MOs) after localization according to the procedure of Boys.[34] The lone pair MO was identified as the highest MO consisting almost exclusively of metal ion functions, the composition of which can be expressed in terms of the different basis functions: s, p, and d. With such analysis, the structural nature of the lone pair can be deduced based on the characteristics of its basis functions.

2.1. Simulation Protocol. A pre-equilibrated elementary cubic box with a side length of 31.14 Å containing one ion (with which the QM region is centered) immersed in 1000 water molecules (ρ = 0.997 g/cm^3) obtained from a QM/MM MD simulation was utilized as a starting configuration. The simulation was run over a canonical ensemble with the temperature (~298 K) maintained via the Berendsen algorithm.[35] A predictor-corrector algorithm was used to integrate the Newtonian equations of motion, with the chosen time step of 0.2 fs to allow explicit hydrogen movements for the flexible BJH−CF2 water model.[32,33] The simulation was sampled for 12 ps after 4 ps of re-equilibration. The total radius of the QM region (core + layer) was set to 5.7 Å. The splitting of the QM region at a radius of 3.5 Å ensures the inclusion of the full first hydration shell into the core region. The smoothing function (eq 1) was applied in the region from 5.5 to 5.7 Å.

3. Results and Discussion

3.1. Structure. The radial distribution functions for Sb−O and Sb−H are shown in Figure 2. Like in the case of Sn(II), the strong shoulder seen in the first shell peak is indicative of non-regular hydration. Following the method for cluster centroid computation described earlier, the system was partitioned to properly reveal any inherent asymmetry. With the use of a Gaussian centered at an Sb−O distance of 2.18 Å (corresponding to first shell maximum of the Sb−O RDF) and having a spread of b = 0.5, the cluster centroid, Q, was generated for each frame of the trajectory. Plane-wise decomposition of the coordinate space using Q as basis leads to the resolution of the Sb−O RDF shown in Figure 3. The presence of two primary binding dispositions, one centered at a distance of ~2.18 Å and another at ~2.70 Å, validates the utility of the centroid computation, and for the remainder of this paper the terms "proximal" and "distal" will be used to refer to the domains of space that corresponds to these primary coordination distances, respectively. In a manner similar to that presented by Marx et al. for the solvation

(24) Frick, R.; Pribil, A. B.; Hofer, T. S.; Randolf, B. R.; Bhattacharjee, A.; Rode, B. M. *Inorg. Chem.* **2009**, *48*(9), 3993–4002.
(25) Azam, S. S.; Hofer, T. S.; Bhattacharjee, A.; Lim, L. H. V.; Pribil, A. B.; Randolf, B. R.; Rode, B. M. *J. Phys. Chem. B* **2009**, *113*(27), 9289–9295.
(26) Hofer, T. S.; Tran, H. T.; Schwenk, C. F.; Rode, B. M. *J. Comput. Chem.* **2004**, *473*, 211–214.
(27) Guàrdia, E.; Laria, D.; Martí, J. *J. Mol. Liq.* **2006**, *125*, 107–114.
(28) Martí, J.; Guàrdia, E.; Gordillo, M. C. *Chem. Phys. Lett.* **2002**, *365*, 536–541.
(29) Stillinger, F. H. *Science* **1980**, *25*, 451–457.
(30) Luzar, A.; Chandler, D. In *Hydrogen Bond Networks*; Kluwer Academic Publishers: The Netherlands, 1994.
(31) Chanda, J.; Chakraborty, S.; Bandyopadhyay, S. *J. Phys. Chem. B* **2006**, *110*, 3791–3797.
(32) Stillinger, F. H.; Rahman, A. *J. Chem. Phys.* **1978**, *68*(2), 666–670.
(33) Bopp, P.; Jancso, G.; Heinzinger, K. *Chem. Phys. Lett.* **1983**, *98*, 129–133.
(34) Boys, S. F. *Rev. Mod. Phys.* **1960**, *32*, 296–299.
(35) Berendsen, H. J.; Grigera, J. R.; Straatsma, T. P. *J. Phys. Chem.* **1987**, *91*, 6269–6271.

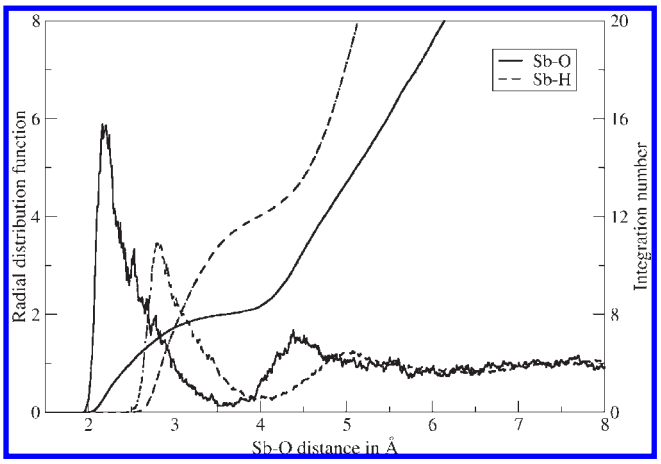

Figure 2. Sb−O and Sb−H radial distribution functions.

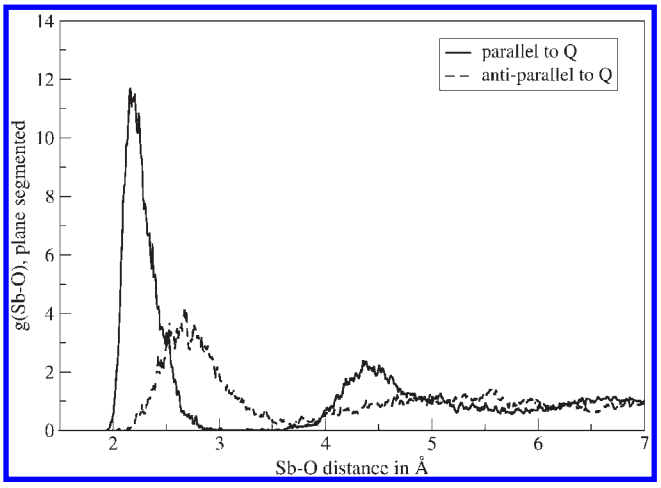

Figure 3. Plane segmented Sb−O radial distribution functions for the hemisphere on the side of the orientation vector (parallel to Q), and for the hemisphere on the opposite side (antiparallel to Q).

of Pt(II) and Pd(II) ions in aqueous solution,[36] the Sb−O radial distribution function was decomposed into angular components. By defining several conical selections spanning up to 180° from the pole axis defined by Q, it was possible to obtain topological representations of varying ligand density around the ion (Figure 4) for a preliminary appraisal of the general shape of hydration.

The exploration of the underlying solvation properties leading to the strongly uneven distribution seen in Figure 4(a) and the reduction of the ligand density in the second shell region at the distal side starts with the elucidation of structural attributes in the first hydration shell. When the radial minimum of 3.6 Å is chosen to mark the boundary of the first hydration shell, the computed average coordination number for the first shell is 8 and the O−Sb−O angular distribution function in this region (Figure 5) indicates a structure based on the square antiprism where typical average angles of 74° and 140° can be observed. The overall coordination number distribution spans from 6 to 9 for the first shell (Figure 6(a)), and 7 to 18 (Figure 6(d)) with an average of 12.2 for the second shell. Surprisingly, while the plane-wise coordination number distributions in the first shell are closely similar (Figures 6(b) and (c)), the second shell distributions for the proximal and distal sides show a remarkable difference in both the spread of coordination numbers and the corresponding averages (Figures 6(e) and (f)). The average coordination numbers for each of the investigated regions are listed in Table 3.

Together with the close proximity of the Sb−H and the distal Sb−O first shell maxima (2.8 Å and 2.7 Å, respectively), the considerable reduction of the second shell peak, and the corresponding average coordination number at the distal spatial partition (Figures 6(f)), suggests that aside from an asymmetric primary hydration, complex interaction dynamics are in place between first and second shell water molecules. In the absence of perturbations to the electron density around the metal ion, solvation dynamics would be guided by symmetric Coloumbic and non-Coloumbic interactions that are isotropic and continuous. Such a scenario would not be expected for a metal ion having a lone electron pair. The stereochemical activity of the lone electron pair on divalent group IV and trivalent group V metal ions has long been regarded as playing a significant role in determining the coordination geometries of complexes for these metal ions,[37,38] albeit in no strict trend. Studies of the kind presented in this work offer the advantage of observing the basic coordination characteristics of metal ions at the molecular level and devoid of dependence on synthetic pathways. The availability of pertinent microscopic information lends the system to copious examination of both structural and dynamical effects. This work therefore attempts to explore the apparent anomalies from the perspective of solvent reorganization.

Computation of the local density corrected three-body distribution functions [23] provides a means of elucidating solvent organizational motifs. This is certainly of interest as despite the apparent diffuse nature of the primary hydration layer (as seen from the Sb−O RDF in Figure 2), the strong Coloumbic interaction of the solvent with the ion would necessarily induce an average global geometry. We therefor give particular attention to the elucidation of structural patterns that relate to the ligand density distribution observed in Figure 4(a). The local density corrected three-body distribution function for the total first shell shows two peaks at ~2.85 Å and ~4.6 Å (Figure 7), indicative of two major triangle populations. The proximal and distal domains of the first hydration shell were analyzed separately. For comparison, the O−O radial distribution function of pure water from QMCF MD simulations[23] is overlaid over the three-body distribution functions. At first glance, one can easily see a remarkable difference between the structural patterns of the proximal and distal domains: the latter showing more semblance to neat water, and the former showing a fairly high degree of structure. The major peak (at ~2.85 Å) in the total first shell distribution appears to be reflected in either hemispherical domain. It is heightened in the proximal domain at 2.75 Å, giving an impression of a relatively stable configuration that is present in this

(36) Beret, E. C.; Martínez, J.; Pappalardo, R. R.; Marcos, E. S.; Doltsinis, N. L.; Marx, D. *J. Chem. Theory. Comput.* **2008**, *4*, 2108–2121.

(37) Emeléus, H. J.; Sharpe, A. G. *Advances in Inorganic Chemistry and Radiochemistry*; Academic Press, Inc.: Orlando, FL, 1985.

(38) Cotton, F. A.; Wilkinson, G.; Murillo, C. A.; Bochmann, M. *Advanced Inorganic Chemistry*, 6th ed.; Wiley-Interscience: New York, 1999.

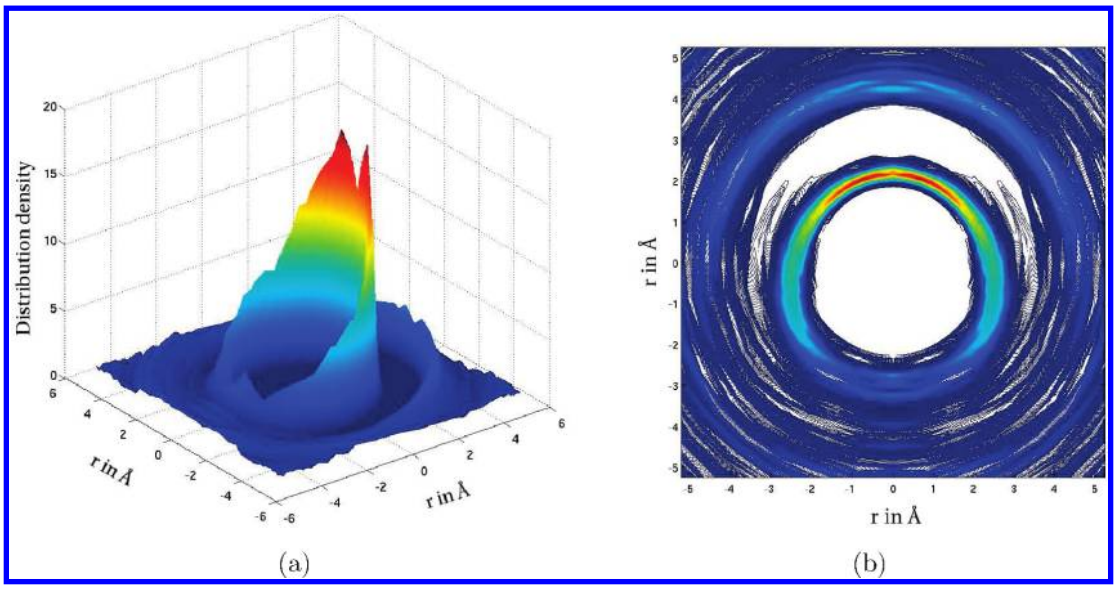

Figure 4. (a) Surface plot of the Sb−O radial-angular density distribution up to 5.6 Å with (b) corresponding contour map showing the general shape of the first hydration shell. Color keys: blue = low density; red = high density.

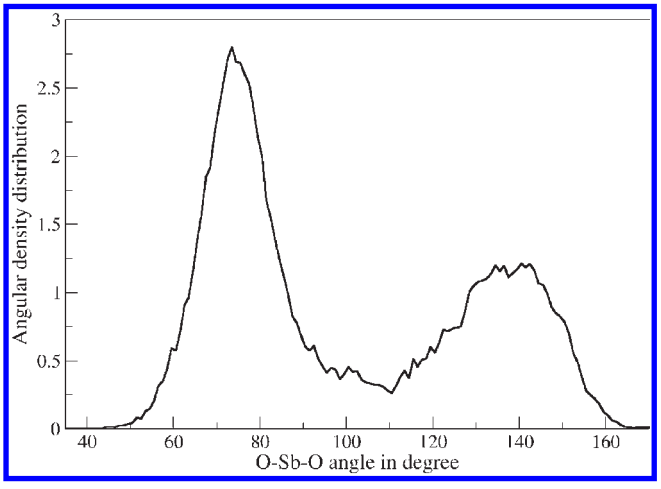

Figure 5. O−Sb−O angular density distribution for the total first shell.

region. The peak position, in conjunction with the Sb−O first shell proximal peak maximum of 2.18 Å, implies an O−Sb−O angle of 78° forming a triangular face in a square pyramidal half of an antiprismatic configuration. On the other hand, the distal domain expresses an attenuated major peak with a wide distribution, indicative of increased lability. The slight shift in relation to the O−O radial distribution (pure water) suggests that the water ligands in this region have been drawn farther from one another, and the association of water molecules may even be weaker than in the bulk. A possible explanation for this is that a "void" is being created to accommodate the lone electron pair in this region. One can imagine that the introduction of the small "void" space would allow increased mechanical freedom for the water molecules in the distal domain leading to a decrease in ligand density. With regard to the minor peak (~4.6 Å) in the total first shell distribution, the fact that neither of the hemispherical domains reflect this feature implies that this distance represents O−O dispositions that cross hemispheres. This feature is fairly weak because of the high degree of lateral fluctuation induced by the lone pair. The net result of solvent reorganization is the "egg-shaped" hydrate complex shown in Figure 4(b). In the succeeding section, we shall discuss what these aforementioned structural features mean in terms of the dynamical characteristics of solvent molecules around the ion.

3.2. Dynamics. Given that the distal domain appears to express little degree of structure beyond that which is native to neat water, we continue by inspecting the dynamic aspect of solvent reorganization. In the case of the solvent experiencing a strong positive charge, strong alignment of water molecules in the first hydration layer would be expected to facilitate the formation of a second hydration layer via the formation of intershell hydrogen bonds. At this point, we temporarily digress from the notion of structure-breaking and structure-forming propensities and simply utilize the premise for explaining the consequence of the apparent distinct hydration domains of Sb^{3+}. Naturally, if the effect of the positive charge of the ion on the dipole of water is diminished in some way, water molecules would gain a higher degree of reorientational freedom. This is the case that can be imagined with the screening effect created by each hydration layer on succeeding solvent regions. Figure 8 shows the different normalized time correlation functions of $\mu(t)$ in a 1 ps window for all regions of interest. As expected, different decay behaviors are present. Most notable is the apparent decay behavior for the first shell distal domain and how it closely compares with that of the second shell proximal domain, thus indicating the effect of the lone electron pair on Sb^{3+} in relaxing the interaction of water dipoles with the ion. The corresponding patterns of the relaxation dynamics of intermittent hydrogen bonds, computed over a region that sufficiently envelopes the first and second shell peak maxima in the radial distribution functions, is shown in Figure 9. Because the computation of $C_{HB}(\tau)$ is indiscriminately applied to all water pairs within the specified volume region, Figure 9 implies that the intermittent hydrogen bond relaxation dynamics observed in the full spherical volume space is almost solely arising

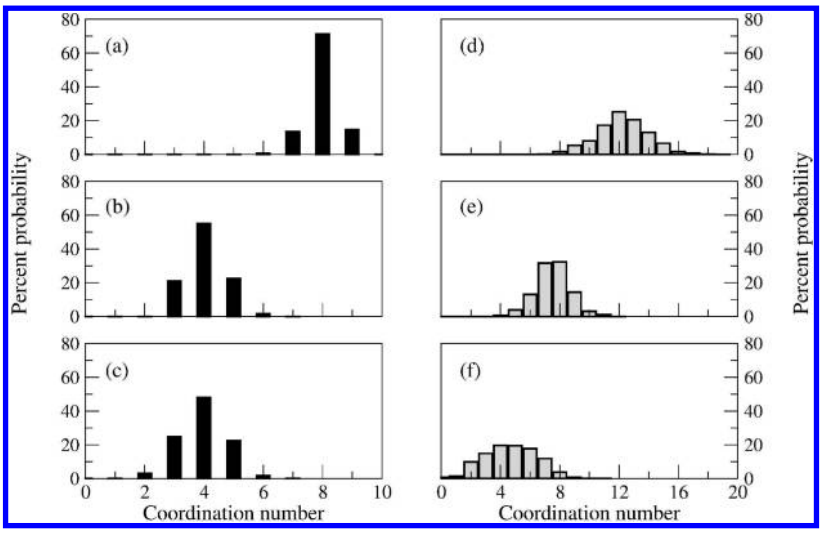

Figure 6. Coordination number distributions for the first shell: (a) overall, (b) proximal domain, (c) distal domain, and for the second shell: (d) overall, (e) proximal domain, (f) distal domain.

Table 3. Average Coordination Numbers for the First (CN^1_{ave}) and Second (CN^2_{ave}) Shell, Total, Proximal, and Distal Regions

region	CN^1_{ave}	CN^2_{ave}
total	8.0	12.2
proximal	4.0	7.5
distal	4.0	4.7

from water pairs belonging to the proximal domain. On the other hand, intermittent hydrogen bond formation-breakage in the distal domain follows a different and faster short time decay and may be solely due to the formation of pairs almost exclusively within first or second shell regions and not pairs that bridge between hydration shells.

The different decay patterns observed in $C_\mu(\tau)$ and $C_{HB}(\tau)$ are consistent with results of the local density corrected three-particle correlations. Thus, the observed degrees of structuring (or its absence) in the different regions can be directly related to a loss (or gain) of reorientational freedom which enforces (or diminishes) intershell hydrogen-bonding. The relaxation times extracted from the long time portion of each of the decay

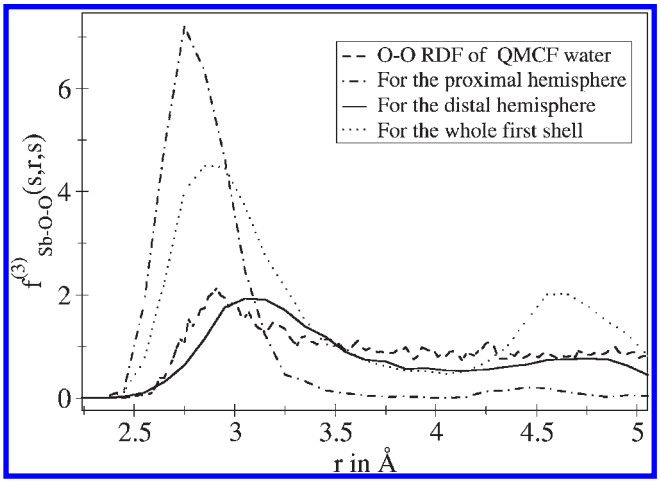

Figure 7. Local density corrected three-body distributions for the first shell for proximal water ligands, distal water ligands, and the O−O radial pair distibution obtained from QMCF water.

curves along with the mean residence times per total hydration shell are listed in Table 4. The relaxation time for dipole reorientational motion ($\tau_{1\mu}$) for the entire first shell (4.8 ps) split into uneven contributions from its proximal and distal domains. This is reasonable, as the water molecules in this region are mostly influenced by the electron density around the ion. Water molecules in the second shell, being farther from the ion and interacting directly with the first shell water molecules instead, have reorientational relaxation times ($\tau_{2\mu}$) that are closer to each other, but follow the same trend observed in the first shell. The corresponding intermittent hydrogen bond relaxation times (τ_{HB}) also convey the same domain-wise trend. The mean residence time for second shell ligands exceeds that of pure water (cf. Table 4), which suggests a general structure-forming ability of Sb^{3+} beyond the first shell. However, the structural patterns observed from the three-body distribution functions imply that this is not the case as far as the hemispherical domains are concerned, particularly because the residual electron density on Sb^{3+} appears to induce a structure-breaking effect on the distal domain of the total hydration volume. The computed relaxation times, τ_μ and τ_{HB}, seems to confirm this picture.

For each of the different relaxation curves, the steep initial decay is suggestive of fast oscillatory motion which overlaps with the diffusional regime to give gradual decay toward longer times. Thus, $\tau_{1\mu}$ appears to be comparable to τ^1_{MRT}. On the other hand, hydrogen bond lifetimes seem to be primarily dictated by second shell dynamics with the proxmity of the values of τ_{HB} with those of $\tau_{2\mu}$, suggesting that a relatively large population of hydrogen bonds come from donors from the second shell region, albeit no definite conclusions can be drawn. Nevertheless, the time correlation functions $C_\mu(\tau)$ and $C_{HB}(\tau)$ readily convey the variability in ligand dynamics between the two domains of interest.

3.3. Stereochemical Activity of the Lone Electron Pair on Sb(III). Finding the connection between the coordination structure and the underlying electronic properties of metal ion complexes is not a trivial task. This is particularly true with metal ion centers possessing a lone electron

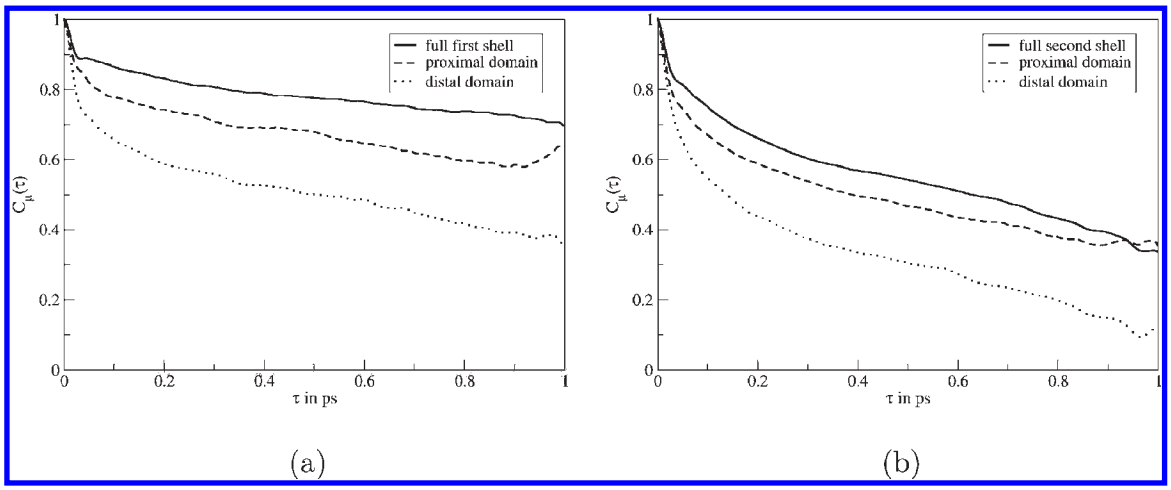

Figure 8. $C_\mu(t)$ for the water molecules in the (a) first, and (b) second hydration shell.

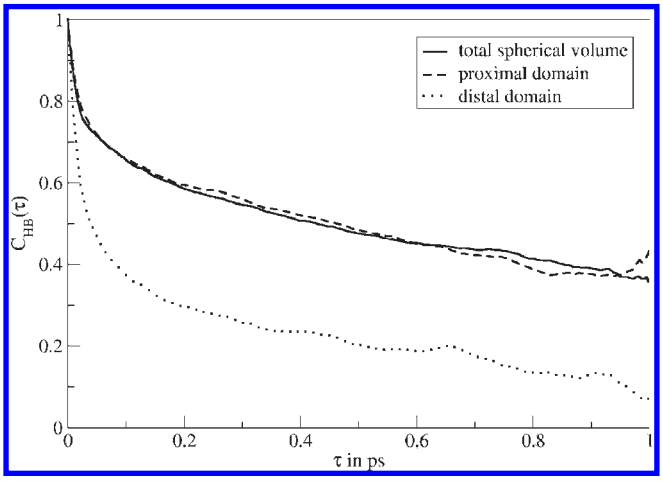

Figure 9. $C_{HB}(\tau)$ for the total first-second shell spherical envelope and for the corresponding proximal and distal domains.

Table 4. Dipole Re-Orientational Relaxation Times for the First ($\tau_{1\mu}$) and Second ($\tau_{2\mu}$) Shell, the Intermittent Hydrogen Bond Relaxation Times (τ_{HB}), and the Mean Residence Times for the Total First (τ^1_{MRT}) and Second (τ^2_{MRT}) Shell[a]

region	$\tau_{1\mu}$ (ps)	$\tau_{2\mu}$ (ps)	τ_{HB} (ps)	τ^1_{MRT} (ps)	τ^2_{MRT} (ps)
Total	4.8	1.4	1.6	5.9	1.7
Proximal	2.8	1.3	1.4		
Distal	1.7	0.8	0.8		

[a] For pure water, the QMCF MD method produces a τ_{MRT} value of 1.2 ps.

pair. The results presented thus far qualify the stereochemical activity of the lone electron pair on Sb^{3+} in the hydrate complex based on structural and dynamical features. However, the predictability of this behavior may not be straightforward for all compounds/complexes of antimony. A modest survey of complexes of antimony with O-bearing ligands is presented in Table 5. With the exception of [SbI_3(thf)], all of the listed complexes exhibit considerable stereochemical activity of the lone electron pair on Sb^{3+} and have hemidirected coordination structures. The results of our simulation appears to be most comparable with antimony triacetate [39] in terms of Sb−O

Table 5. Stuctural Parameters Obtained from Either XRD or EXAFS for Select Antimony Complexes[a]

complex	CN	$R_{Sb\text{--}O}$, Å	reference
antimony triacetate	7 + e	$2.06_{(sh)}$, $2.60-2.78_{(lo)}$	39
$Sb(thd)_3$	6 + e	$2.055-2.065_{(sh)}$, $2.441-2.468_{(lo)}$	40
$Sb(OEt)(thd)_2$	5 + e	$1.923-2.089_{(sh)}$, 2.346, $2.395_{(lo)}$	40
$Sb(OH)_{3,neu}$	3.6	1.96	41
$Sb(OH)^-_{4,\ bas}$	4	1.98	41
$Sb(OH)^+_2\ 2H_2O_{,aci}$	4	1.96, 2.22	41
Sb^{III}−tartrate	4	2.02, 2.22	41
$[Sb(pydc)(H_2O)]_2O$	5	1.89−2.49	42
[SbI_3(thf)]	6	2.85, 3.020	51

[a] CN = number of coordinated atoms to antimony; an e is appended whenever the lone pair has been explicitly considered in the coordination polyhedra. Subscripts $_{(sh)}$ and $_{(lo)}$ indicate *short* and *long* Sb−O distances, respectively, whenever they have been explicitly noted in the reference. *neu, bas, aci* correspond to neutral, basic, and acidic aqueous media respectively.

bond distances. Indeed, the predicated secondary bonding at $2.60-2.78_{(lo)}$ Å can be easily related to the observed distal domain Sb−O distance in our simulations (2.7 Å). On the other hand, the value of 2.18 Å observed in the proximal hemisphere of the Sb^{3+} hydrate reflects the short Sb−O bond distances found in antimony triacetate,[39] $Sb(thd)_3$,[40] $Sb(OEt)(thd)_2$,[40] Sb^{III}−tartrate,[41] and $[Sb(pydc)(H_2O)]_2O$.[42] The different hydroxide species proposed by Tella et al., $Sb(OH)_3$, $Sb(OH)_4^-$, $[Sb(OH)_2]^+(2H_2O)$,[41] offer insight into the fate of proximally bound water molecules to Sb^{3+}, with the neutral $Sb(OH)_3$ species being the most likely product if the simulation had been allowed to run sufficiently longer (in contrast to As^{3+}, which was found to hydrolyze nearby water molecules in less than 200 fs [43]).

The regular octahedral geometry around Sb in polymeric [SbI_3(thf)] along with other examples of symmetric complexes of Sb (e.g., $(NH_4)_2SbBr_6$,[38] *N*,*N*′-dimethyloxamide antimony(III) cloride [44]), imply that empirical

(39) Hall, M.; Sowerby, D. B. *J. Chem. Soc., Dalton Trans.* **1980**, 1292–1296.
(40) Horley, G. A.; Mahon, M. F.; Mazhar, M.; Molloy, K. C.; Haycock, P. W.; Myers, C. P. *J. Chem. Soc., Dalton Trans.* **2002**, 4416–4421.
(41) Tella, M.; Pokrovski, G. S. *Geochim. Cosmochim. Acta* **2009**, *73*, 268–290.
(42) Abboud, K. A.; Palenik, R. C.; Palenik, G. J.; Wood, R. M. *Inorg. Chim. Acta* **2007**, *360*, 3642–3646.
(43) Bhattacharjee, A.; Hofer, T. S.; Pribil, A. B.; Randolf, B. R.; Rode, B. M. *Chem. Phys. Lett.* **2009**, *473*, 176–178.
(44) Wandiga, S. O. *Pure Appl. Chem.* **1999**, *71*, 1019–1024.

evidence of the stereochemical activity of the lone electron pair on Sb^{3+} may be subject to several qualifications. For example, by steric considerations, low coordination numbers for the complexes make it possible for the lone pair to be accommodated in one of the open vertices of an enclosing polyhedron. However, the existence of 6-coordinated complexes with regular octahedral configurations appears to be in contradiction to the 8-coordinated hydrate complex in the present work and with the 7-coordinated acetate complexes,[39] both of which have highly irregular geometries. The regular octahedral geometries of $(NH_4)_2SbBr_6$, *N*,*N*′-dimethyloxamide antimony(III) cloride, and triido(tetrahydrofuran-*O*)-antimony(III), all seem to be explainable according to a generally accepted trend that stereochemical activity of the lone pair in the complex decrease in the presence of "soft" ligands (e.g., halides).[38,45] This may be due to the fact that "soft" ligands are likely to form more covalent interactions with the ion, which enforce regular geometries to minimize repulsion between electron densities of adjacent bonds. Thus, the presence of the large iodine atoms also explains the large Sb−O bond distances in SbI_3(thf). The situation is different in aqueous solution as the interaction of the ion with water molecules is essentially Coulombic. Higher coordination structures (CN > 8) for Sb^{3+} in solution may be expected to push configurations to more regular geometries by steric effects, but this is difficult to substantiate because of the high thermal disorder in the liquid state, which would obscure the distinguishability of RDF peak positions.

Ultimately, any rationalization of the coordination structure of the complex must properly include electronic attributes into account. The nature of the lone pair is often related to *s* and *p* orbital characteristics with hemidirectional coordination originating from a high degree of the latter. Inspection of MOs of selected hydrate structures from our simulation showed the contributions of symmetric *s* functions, and directional *p* and *d* functions to the lone pair MO, respectively, as 29.0%, 14.8%, and 56.2%. It is apparent from this composition that *d* functions are also involved in determining the structural properties of the lone electron pair. Mixing of spherical *s* functions with considerable contributions of *p* and *d* functions would make the lone pair on Sb^{3+} in the hydrate complex essentially lobular. Because the simulation has explored conditions prior to hydrolysis, the strong Coloumbic interaction of the water molecules with the ion appears to have traced this lobular electron density around Sb^{3+} (Figure 4(b)). Such a prominent spatial feature of the lone electron pair would be less likely to manifest itself if it had occupied a valence *s* orbital that is more contracted and stabilized by relativistic effects. This would be the case for heavier metal ions. Bi(III), for example, shows little to no stereochemical activity for its lone pair.[38,46,47] The considerable stabilization of the valence *s* orbital may explain why the heavy Pb^{2+} ion was found to have a holodirected hydrate complex,[48] although this cannot be concluded as a governing factor for all complexes of lead.

The reasons by which the stereochemical activity of the lone pair on antimony arises is still to be unequivocally established and would require more investigations similar to those performed by Takeda et al. for sulfur and halide complexes of antimony.[49] With the structural diversity of its compounds/complexes, lead seems to offer a comparable analogue to antimony in terms of the functionality of the lone electron pair, and several trends may be seen to be common in both.[45,50] For example, the hemidirectional behavior of the 8-coordinated Sb^{3+} hydrate complex seems reasonable if noted with regard to the 7- and 8-coordinated hemidirectional structures of divalent lead compounds, found in the Cambridge Structural Database, that have a signicant number of Pb−O bonds.[50] In view of literature data and the results of the present work, we find a consensus for the rationalization of the stereochemical activity of the lone electron pair on Sb^{3+} (which may be extended to other group IV and V metal ions) based on the following factors: (1) the electronic composition of the lone electron pair, (2) the nature of ligand atoms, and (3) steric effects. Because the first of these factors is most conveniently explored via computational methods, we believe that the convergence of theory with experiments promises a thorough understanding of the properties of complexes having metal ion centers with a lone electron pair.

4. Conclusion

Altogether, the results that have been presented demonstrate the utility of invoking quantum mechanical treatment in describing many-body interactions that are inherently susceptible to electronic effects. Like its isoelectronic counterpart, Sn^{2+}, the Sb^{3+} ion seems to possess a high capability of partitioning its hydration volume into distinct domains having very different structural and dynamical characteristics. Although it is possible to model such unique behavior using complex multipolar force field expansion schemes, the ab initio QMCF MD framework offers a more straightforward, unbiased approach to capturing the behavior of the lone electron pair on the Sb^{3+} ion while maintaining a good compromise between speed and accuracy.

Complex interaction patterns arising from the presence of residual electron density have long been of interest from both theoretical and experimental perspectives. Despite having a relative large number of surrounding water ligands, a hemidirectional coordination environment around the Sb^{3+} ion was confirmed through detailed structural and dynamical analyses. The distinct hydration domains in the first shell region equally maintain an average of 4 ligands, but have average Sb−O distances that were found to be different: one being closer for those that are more stably bound (2.18 Å),

(45) *Progress in Inorganic Chemistry*; Karlin, K. D., Ed.; Wiley-Interscience: NJ, 2003; Vol. *51*.
(46) Hill, N. J.; Levanson, W.; Patel, R.; Reid, G.; Webster, M. *J. Chem. Soc., Dalton Trans.* **2004**, 980–981.
(47) Näslund, J.; Persson, I.; Sanström, M. *Inorg. Chem.* **2000**, *39*, 4012–4021.
(48) Bhattacharjee, A.; Hofer, T. S.; Pribil, A. B.; Lim, L. H. V.; Lichtenberger, A.; Rode, B. M. *J. Phys. Chem. B* **2009**, *113*(39), 13007–13013.
(49) Ohyama, R.; Takahashi, M.; Takeda, M. *Hyperfine Interact.* **2005**, *161*, 99–111.
(50) Shimoni-Livny, L.; Glusker, J. P.; Bock, C. W. *Inorg. Chem.* **1998**, *37*, 1853–1867.
(51) James, S. C.; Norman, N. C.; Orpen, A. G.; Quayle, M. J. *Acta Crystallogr.* **1997**, *C53*, 1024–1027.

and another being farther (2.70 Å) for those that are loosely bound. This particular feature of the Sb^{3+} hydrate complex implies that a balance is made between the provision of a small "void" volume to accommodate the lone electron pair and the strong electrostatic interaction of oxygen centers of water with the ion, which allows high coordination states. The consequence of the uneveness in ligand distribution becomes more apparent when viewed in the context of solvent reorganizational patterns and molecular motion. Furthermore, spatial decomposition of the three-dimensional coordinate space has allowed extraction of more detailed information on hydration properties that are often inaccessible or are masked in purely radial sampling averages.

Acknowledgment. Financial support from the Austrian Science Foundation (FWF) and an ASEAN-European Academic University Network technology grant from the Austrian Ministry of Science and Research are gratefully acknowledged.